Journal of Computational Science &Engineering 45 (2020) 1103-1119

Available at http://www.asocse.org ISSN 1710-4068

Relationship between the structure and toxicity of Metal Oxide Nanoparticles

Yuting Gao[1], Xiaokang Chen[1], Honglin Zhai[2], Xilin She[3], Hongzong Si[4*]

[1]Department of Data Science and Software Engineering,Qingdao University Medical College,266071, China

[2]College of Chemistry and Chemical Engineering, Lanzhou University, Lanzhou,730030, China

[3]School of Environmental Science and Engineering, Qingdao University, Qingdao, 266000, China

[4]Institute for Computational Science Engineering, Qingdao University, Qingdao, 266071, China

Abstract: **The nanomaterials posed risks to human health. There is a need for simple and effective methods to predict the toxicity of unknown nanoparticles. Quantitative structure-activity relationships were used to research the toxicity of metal oxide nanoparticles. 25 descriptors of 21 metal oxide nanoparticles were obtained. It is found that the toxicity is related to 5 descriptors including χc, Shift, E_g, ZPVE, and Softness by using the multiple linear regression method with an R^2 of 0.893. Structures of two metal oxide (silver oxide and lead oxide) nanoparticles were designed based on multiple linear regression equation. And we found the structural models of them with the lowest toxicity. The multiple nonlinear regression model was used to further improve the prediction accuracy. The R2 were 0.943 in training set and 0.931 in test set, which indicated that the prediction accuracy has been improved effectively. Based on the results, we explained the effects of the 5 descriptors on toxicity, discussed the mechanism of toxicity of metal oxide nanoparticles, and proved that reactive oxygen species is an important cause of the toxicity. Finally, it is concluded that the quantitative structure-activity relationships model is a reasonable method to design the structures of metal oxide nanoparticles with lower toxicity.**

Keywords: DFT; Metal oxides; Nanoparticles; QSAR; Toxicity

Received 5 January 2020, Revised 17 February 2020, Accepted 20 February 2020

*Corresponding Author: Hongzong Si, sihz03@126.com

1. Introduction

Large quantities of products of nanotechnology are mass-produced. They have been applying in almost all fields of human life [1] [2] [3]. They are called nanomaterials (NMs) [4]. Metal oxide NMs are accounted for a large part [5]. These metal oxide NMs have been used in microelectronics, paints, textiles and cosmetics [6]. The toxicity of NMs has become a key factor limiting the development. Currently, many researchers have studied the toxicity of metal oxide nanoparticles (NPs) [7]. Minigalieva et al. [8] found that both pulmonary and systemic toxicity of CuO, PbO and ZnO NPs to rats, which revealed that metal oxide NPs were toxic to organisms [9]. Therefore, it is significant to study the toxic mechanism of metal oxide NPs and predict its toxicity.

1.1. Toxicity Mechanism of Metal Oxide NPs

1.1.1. The influence of particle size

Metal oxide NPs can enter cells easily through cell membranes due to their small particle sizes. Moreover, Metal oxide NPs with smaller particle size has a larger specific surface area, which leads to an increase in the contact area between NPs and cells. These are two reasons for the high toxicity of metal oxide NPs. Baek et al. [10] studied the toxicity of CuO, NiO, ZnO and Sb_2O_3 NPs to escherichia coli, bacillus subtilis and streptococcus aureus. They concluded that the large specific surface area and surface structures of metal oxide NPs were important factors determining the toxicity. H. L. Karlsson et al. [11] compared the toxicity of nanoscale and micron-scale particles of certain metal oxides (Fe_2O_3, Fe_3O_4, TiO_2 and CuO). The study found that the CuO NPs were much more toxic compared to CuO micrometer particles. One key mechanism may be the ability of CuO to damage the mitochondria. In contrast, the micrometer particles of TiO_2 caused more DNA damage compared to the nanoparticles, while The Fe_2O_3 and Fe_3O_4 showed no clear difference between the different particle sizes. Therefore, it can be concluded that particle size is not the only key factor affecting the toxicity of metal oxide particles.

1.1.2 The influence of reactive oxygen species (ROS)

Many studies indicted that oxidative stress induced by ROS is one of the most important toxic mechanisms of metal oxide NPs. Liu et al. [12] studied the toxicity of carbon nanotubes (CNTs) to lungs and proved that CNT-induced oxidative stress was regarded as the most acceptable mechanism. ROS produced by oxidative stress can react with cellular macromolecules including DNA, proteins and lipids. Furthermore, ROS can disturb the homeostasis of the intracellular milieu. These proved that CNTs may cause DNA damage indirectly by promoting oxidative stress and inflammatory responses. A. Semisch et al. [13] found that the reason why copper oxide NPs had high toxicity to A549 cells might be caused by copper ions distributed inside and outside the cells. These reasons might be related to the formation of excessive ROS. And Chairuangkitti et al. [14] studied the toxicity of silver NPs to lungs, and found that silver NPs caused ROS formation in cells, and then further caused a decrease in mitochondrial membrane potential in their

2019@ The American Computational Science Society. All rights reserved.

cell viability and mitochondrial membrane potential. As a result, the proportion of cells in the apoptotic population increased. In addition, some researchers believed that the toxicity of metal oxide NPs may be related to the surface charge distribution [15]. These metal oxide NPs have large surface area, and the charges are not uniform. If the surface charge distribution is denser, the redox ability is stronger. This will generate more ROS, and the biological toxicity effect of metal oxide NPs would be higher.

After research, we concluded that metal oxide NPs can induce cellular oxidative stress, reduce cell activity, and induce cell apoptosis, which are important causes of the toxicity. For example, the valence state transition of the metal cations released from the metal oxide NPs in cells can change the redox metabolites, destruct the redox balance, and play an important role in the formation of cytotoxicity. In addition, after these metal oxide NPs enter the cells, the generated metal ions may induce excessive ROS production, and lead to cytotoxicity. There are many sources of ROS in the cells. For example, the normal metabolism of cells, the activity of metal oxide NPs and the metal ions with redox activity in the cytoplasm can induce the production of ROS. It is generally accepted in the academic community that excessive levels of ROS could induce oxidative stress and inflammatory reactions. This process further increased the formation of ROS. For example, intracellular Fe^{2+} can induce the hydroxyl radical production through the Fenton reaction, which may lead to DNA oxidative damage. Metal cations released into cells often target a negatively charged DNA molecule and interact with it. The binding of metal cations to DNA can cause DNA structural changes, further causing DNA damage, and resulting in genotoxicity [16]. The oxidative stress toxicity of metal oxide NPs can be caused by 2 reasons: (1) nanoscale structure and surface modification affect many cellular biochemical processes; (2) the decomposition of NPs and the release of metal ions interfere with cellular homeostasis severely [17].

The influence of ROS on toxicity is also shown in lipid peroxidation. The specific process of lipid peroxidation is that the ROS generated by metal oxide NPs and the macromolecules such as phospholipids on the cell membrane undergo a free radical chain reaction. The process could lead to lipid peroxidation and finally destroy the cell membrane, thereby showing the cytotoxicity. Wang et al. [18] studied the mechanism of TiO_2 NPs on bacterial toxicity. It was found that the level of MDA in Escherichia coli was increased by ultraviolet radiation. The finding indicated that the generated ROS attacked the polyunsaturated phospholipid on Escherichia coli cell membrane, resulting in lipid peroxidation and caused the cell membrane to rupture. Kim et al. [19] used electron spin resonance to prove that silver NPs generate free radicals and destroy bacterial cell membranes. After adding antioxidant N-acetylcystein to the system, free radicals were reduced. Silver NPs also lost the bacteriostatic effect. These conclusions prove that the ROS generated by metal oxide NPs in cells is an important cause of its toxicity.

1.2. Quantitative structure-activity relationships (QSAR)

As a mathematical model, QSAR can describe the relationship between molecular structure and the biological activity quantitatively by using mathematical models [20]. The basic assumption of QSAR is that the structures contain information which determines the physical, chemical, and biological properties; and these physical and chemical properties further determine the biological activity. Furthermore, the selected descriptors should be related to the biological activity. QSAR has become a hotspot for research because of the simple calculation and good prediction ability. In the case of unknown receptor structures, QSAR is one of the most accurate and effective ways for drug design [21]. According to the results of QSAR, researchers can modify the physiologically active substance purposefully. Researchers got many achievements based on QSAR [22]. For example, Liu et al. [23] studied the toxicity of metal oxide NPs to human bronchial epithelial (BEAS-2B) and murine myeloid (RAW 264.7) cells. They built a prediction equation based on 2 descriptors, namely conduction band energy (E_C) and ionic index ($Z_{2/r}$). Hu et al. [24] found the cytotoxicity of metal oxide NPs was correlated with cation charges after regression calculation based on QSAR model.

1.3. Combination of theoretical calculation and QSAR

While people have achieved success with QSAR, how to further simplify the research process and improve the prediction accuracy became the focus of QSAR development [24]. And theoretical calculated method based on the density functional theory (DFT) and the first principles met the requirements. Current mainstream theoretical calculated methods include Vienna Ab-initio Simulation Package (VASP) and Gaussian [25]. VASP is mainly used for the calculation of periodic structures, such as crystals. Gaussian is mainly used for the calculation of aperiodic structures, such as clusters and nanoparticles. In the article, As the structures of metal oxide NPs were non-periodic, so Gaussian was selected as the theoretical calculation method. A. Soffers et al. [26] tried to improve the predictive ability of QSAR by defining more descriptors based on theoretical calculations and describing QSARs by multi-parameter approaches. In the combination of theoretical calculation based on density functional theory and QSAR (DFT-QSAR) method, Molecular models are constructed in specialized chemical software, and a series of descriptors are calculated. Relative to experimental QSAR research, the descriptors are obtained without the need of complex experimental procedures and

2019@ The American Computational Science Society. All rights reserved.

expensive instruments, but using theoretical calculations. The method can save us from experiments. In the experimental QSAR research, there are differences in structures and particle sizes between different compounds/ NPs, and the sources of some descriptors are varied. For example, the experimental environments and instruments are different; and it is difficult to ensure the consistency. In addition, the experimental QSAR research require much time to prepare samples, and the requirements of measuring the descriptors are high for both the instrument and the technical level of researchers. These problems have limited the development of QSAR.

In the article, we used the DFT-QSAR method to study the toxicity of metal oxide NPs, and improved the accuracy of results while saving experimental time and fund.

1.4. Relationships Between Structures and Toxicity

It is well known that it is difficult to explain the relationship between the structure of a compound/ NPs and toxicity. Because it is difficult to determine which structures of the compound/ NPs have a significant effect on toxicity. However, through DFT-QSAR modeling and calculation, we can select several descriptors that have significant effects on toxicity, and study these descriptors to obtain the influence on toxicity.

In the article, X_c, *Shift,* E_g, *ZPVE*, and *Softness* are the 5 descriptors that have significant influence on the toxicity of HaCaT cells based on QSAR model.

(1) X_c is defined as the electronegativity. It is a scale of the ability of atoms to attract electrons, indicating the ability of atoms to attract electrons. The greater the electronegativity, the stronger the ability to attract electrons. and the more likely it is to induce the production of ROS. These ultimately lead to higher toxicity of metal oxide NPs.

(2) *Shift* is defined as half of the sum of the highest occupied orbital energy (E_{Homo}) and the lowest unoccupied orbital energy (E_{Lumo}). The *Homo* orbit has a weaker reaction on the electrons, so it's more likely to lose electrons. *Lumo* orbit has stronger affinity for electrons and is more susceptible to electrons. If the value of *Shift* is larger, the chemistry of the molecule is more active. Therefore, metal oxide NPs would exhibit higher toxicity.

(3) E_g is defined as the difference between the Homo and the Lumo (band gap). It can be used to measure the barrier a molecule has to overcome to enter an excited state. If the value of E_g is larger, the molecules need to overcome larger energy barrier to enter the excited state. In other words, metal oxide NPs has higher stability, which leads to lower toxicity.

(4) *ZPVE* is defined as the Zero-point vibrational energy. It can be seen from (1) that if the value of *ZPVE* is greater, the metal oxide NPs would be less toxic. The reason may be that the toxicity of the metal oxide NPs is related to the ground state energy. If the value of *ZPVE* is smaller, the ground state energy under vacuum and the energy barrier of the electron transition would be lower, and the metal oxide NPs would be more likely to react with the cells to generate ROS, thereby causing an increase in toxicity.

(5) *Softness* is defined as the Chemical softness based on the Hard-Soft-Acid-Base theory (HSAB) [27]. The values of *Softness* were derived from literatures [28]. If the value of softness is large, the charge density is low and the molecular radius is large. Moreover, If the value of *softness* is large, the value of polarity is low, and the toxicity is low. In addition, large value of *softness* correspond to low charge density and large molecular radius, resulting in reduced electron transfer capacity. Therefore, it is less likely to produce ROS. So the toxicity would be low.

In this work, we used the DFT-QSAR method to establish linear and non-linear models to study the toxicity of metal oxide NPs to cells, and clarified the toxicity mechanism of metal oxide NPs. Compared with experimental QSAR, DFT-QSAR has higher accuracy and simpler method. In addition, we designed low-toxic structures of silver oxide NPs and lead oxide NPs based on the QSAR model.

2. Materials and Methods

In the article, 21 kinds of metal oxide NPs were chose as the samples. The median lethal concentration (LC_{50}) value was chose as the descriptor to quantify the toxicity of the 21 metal oxide NPs. To get the results of linear fitting, the natural logarithm value of the negative logarithm of LC_{50} ($\ln(\log_{10}((LC_{50})^{-1}))$) were set as response variables based on Box-Cox transformation. The values of LC_{50} were derived from a series of literatures on cytotoxicity [29] [30] [31] [32]. The international unit of LC_{50} is milligrams per liter (mg/L). To make the data more concise and intuitive for statistics, the unit of LC_{50} in the article is microgram per liter (μg/L). And these data are listed in Table 1.

Table 1. Values Of The LC_{50} And $\ln(\log_{10}((LC_{50})^{-1}))$ Of 21 Metal Oxide Nps

NPs	Molecular formula	LC_{50} (μg/L)	$\ln(\log_{10}((LC_{50})^{-1}))$
Titanium dioxide	TiO_2	7.240	0.761
Aluminum oxide	Al_2O_3	3.801	0.884
Zirconium oxide	ZrO_2	2.630	0.940

2019@ The American Computational Science Society. All rights reserved.

Ferric oxide	Fe_2O_3	3.981	0.875
Silicon dioxide	SiO_2	2.884	0.932
yttrium oxide	Y_2O_3	1.585	1.030
Chromium oxide	Cr_2O_3	8.710	0.723
Antimony trioxide	Sb_2O_3	0.759	1.138
Nickel oxide	NiO	0.162	1.332
Bismuth trioxide	Bi_2O_3	0.282	1.267
Tin oxide	SnO_2	2.951	0.928
Lanthanum oxide	La_2O_3	0.011	1.601
Indium trioxide	In_2O_3	1.479	1.040
zinc oxide	ZnO	0.002	1.756
Cobalt oxide	CoO	0.741	1.141
Vanadium trioxide	V_2O_3	0.331	1.247
Tungsten trioxide	WO_3	2.754	0.940
Manganese oxide	Mn_2O_3	0.002	1.737
Copper oxide	CuO	4.074	0.871
Magnesium oxide	MgO	263.027	-0.536
Calcium oxide	CaO	427.563	-0.997

A total of 25 descriptors including quantum mechanical descriptors and geometric descriptors were calculated and queried. These data were listed in Table 3 and Table 8. These definations of 25 descriptors were listed in Table 9.

First, the average size of the metal oxide NPs was obtained by consulting the literatures and controlled the size below 9 nm. SiO_2 NPs and SnO_2 NPs had 7 metal atoms. WO_3 NPs had 4 metal atoms. And the numbers of metal atoms of the rest of metal oxide NPs were 6. Then these structural models were obtained in the molecular structures library in Materials studio (MS) software. Next, these structural models were imported into GaussView 5.0 software, and were saved as the Gaussian input file (.gjf). Then the Gaussian input files were opened in Notepad++ software. In this step, the memory space, compute node, number of CPU cores and operation base group required by the server group were set manually. The Gaussian input file contents were set to 4500MW of memory space, 2 compute nodes, and 16 CPU cores. B3LYP and LANL2DZ were selected as the operation base groups.

2.1. Multiple linear regression (MLR) analysis

The Gaussian input files of 21 metal oxide NPs were submitted to server for structural optimization and frequency calculation. The detailed steps are as follows: (1) The server is minicomputers with 28 cores. (2) We used Linux language to operate Xshell software to send commands to the server. (3) We used Xftp software to set up file transfers between the local computer and the server. (4) We used the "cd" command to enter the folder where the ".gjf" files were located on the server. (5) We used the "dos2unix" command to convert the Windows format file to the Linux format file. (6) We used the "g09&" command to start gaussian software on the server for optimization and frequency calculation. And 25 descriptors of the 21 metal oxide NPs were obtained in total.

In the MLR model, We adopted a stepwise regression method and a Box-Cox transformation. The Box-Cox transform is an exponential transform that can find the best possible way to keep the data as normal (95% confidence interval). We cannot find the optimal λ because of the stepwise regression. After a lot of experimentation, we decided to set λ to 0, which meaned taking the natural logarithm of the dependent variable. So the values of ln(log10((LC50)-1)) of the 21 metal oxide NPs were set as the response variable. And the values of 25 descriptors were set as continuous predictive variables. Then these data were imported into Minitab software for stepwise regression analysis.

Alpha (A) and alpha (N) represent the maximum risk level for accepting/ rejecting the null hypothesis as true, which are generally 0.05. In this article, we should chose a value slightly greater than 0.05 to increase the probability of detecting false assumptions. On this basis, we tried 0.04, 0.05, 0.06, 0.07, 0.08, 0.09 and 0.100. The results were shown in Table 2. After analyzing the fitting results, when λ is 0.040, the values of R2 was low; when λ was 0.050-0.090, the results were the same; when λ was 0.100, the P value of HOMO was larger than 0.05 and VIF values of Eg and HOMO were larger than 5. These did not meet the statistical requirements. So we decided to set alpha(A) and alpha(N) to median value (0.07). We built the MLR model and got the toxicity prediction equation

2019@ The American Computational Science Society. All rights reserved.

with five descriptors. Finally, the result passed the analysis of variance and significance test, which further proved the rationality of the MLR model.

Table 2. Smmary Of The Results Of Three Values Of Alpha(A) And Alpha(N)

Values of λ	R^2	Selected descriptors	P Values	VIF
λ=0.04	0.603	*Shift*	0.000	1.000
λ=0.05 λ=0.06 λ=0.07 λ=0.08 λ=0.09	0.893	X_c	0.011	1.910
		Shift	0.000	3.630
		E_g	0.001	3.120
		ZPVE	0.009	1.110
		Softness	0.000	1.060
λ=0.100	0.913	*Softness*	0.000	1.120
		Shift	0.000	4.020
		ZPVE	0.004	1.140
		E_g	0.008	33.050
		HOMO	0.097	25.280
		X_c	0.007	1.920

Table 3. Smmary Of The ValuesOf The 5 Descriptors Of 21 Metal Oxide Nps

NPs	X_c	*Shift*	E_g	*ZPVE*	*Softness*
TiO_2	2.632	-0.003	-0.066	151002.400	-0.230
Al_2O_3	2.539	-0.015	-0.172	178830.100	-0.100
ZrO_2	2.506	-0.005	-0.035	217818.000	-0.080
Y_2O_3	2.180	-0.002	-0.166	140628.600	-0.270
Cr_2O_3	2.552	-0.008	-0.072	160106.000	-0.130
Sb_2O_3	2.570	-0.011	-0.075	144161.700	-0.140
NiO	2.797	-0.025	-0.036	69383.300	-0.150
Bi_2O_3	2.563	-0.020	-0.174	139870.300	-0.120
SnO_2	2.780	-0.007	-0.085	231654.800	-0.210
In_2O_3	2.501	-0.005	-0.122	135764.700	-0.130
ZnO	2.852	-0.027	-0.063	60185.700	-0.160
CoO	2.543	-0.030	-0.101	69601.500	-0.190
V_2O_3	2.180	-0.004	-0.092	166807.100	-0.220
Mn_2O_3	2.382	-0.067	-0.071	160417.400	-27.780
CuO	2.557	-0.032	-0.041	58705.400	-0.170
Fe_2O_3	2.672	-0.015	-0.084	167550.300	-0.120
SiO_2	2.827	-0.022	-0.132	264015.200	-0.120
La_2O_3	3.131	-0.006	0.002	95613.800	-0.110
WO_3	2.643	-0.008	-0.050	110977.800	-0.120
MgO	1.855	-0.666	-0.745	141233.400	-0.182
CaO	2.049	-0.356	-0.039	116798.200	-0.286

2.2. Structural designs of two metal oxide NPs with low toxicity

2.2.1. Structural design of silver oxide (Ag2O3) NPs

The method of designing the Ag_2O_3 NPs with low toxicity is to control the values of the related descriptors in MLR equation. The basic approach is to obtain the structure with the lowest toxicity through modeling and theoretical calculations, thereby guiding the synthesis of Ag_2O_3 NPs with low toxicity. The

2019@ The American Computational Science Society. All rights reserved.

specific steps are as follows: Based on MLR analysis, 8 different structural models of Ag_2O_3 NPs were constructed in MS software. The related descriptors of the 8 kinds of Ag_2O_3 NPs were calculated in Gaussian software. These structural models of the 8 kinds of Ag_2O_3 NPs were shown in Table 4. Then these descriptors were put into MLR equation to get the predicted values of toxicity. And the structural model of Ag_2O_3 with the lowest toxicity was found. In addition, the structural model with the lowest toxicity is determined by analyzing the predicted toxicity data of the 8 kinds of Ag_2O_3 NPs.

Table 4. Structural Models Of The 8 Kinds Of Silver Oxide NPs And 8 Kinds Of Lead Oxide NPs

Ag_2O_3	Structural model	PbO	Structural model
No. 1	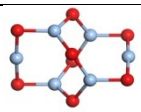	No. 1	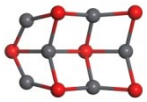
No. 2	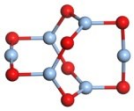	No. 2	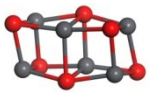
No. 3	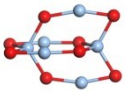	No. 3	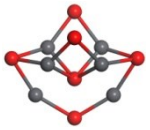
No. 4	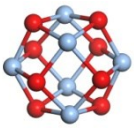	No. 4	
No. 5	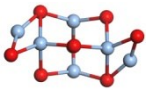	No. 5	
No. 6	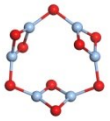	No. 6	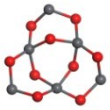
No. 7	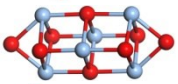	No. 7	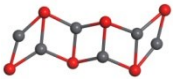
No. 8	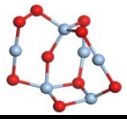	No. 8	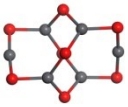

Based on the structural model with the lowest toxicity, the relationship between the toxicity of Ag_2O_3 NPs and the number of silver atoms was further discussed. In the first step, the structural models of Ag_2O_3 NPs with silver atoms of 2/4/6/8/10/12 were constructed in MS software. In the second step, we used Gaussian software to calculate the related descriptors, and the toxicity data were predicted respectively. Finally, the structural model of Ag_2O_3 NPs with the lowest toxicity was determined.

2.2.2. Structural design of lead oxide (PbO) NPs

Similar to the research process of Ag_2O_3 NPs, 8 different structural models of PbO NPs were built in MS software and the related descriptors of the 8 kinds of PbO NPs were calculated. These structural models of the 8 kinds of PbO NPs are shown in Table 4. And the structural model of PbO NPs with the lowest toxicity was found.

Based on the structural model with the lowest toxicity obtained in the previous step, the relationship between the toxicity of PbO NPs and the number of lead atoms was further discussed. The structural models of PbO NPs with lead atoms of 2/4/6/8/10/12 were constructed in MS software, and the related descriptors were calculated in Gaussian software. Then these descriptors were imported into MLR equation to calculate the values of $\ln(\log_{10}((LC_{50})^{-1}))$. Finally, the predicted values of toxicity and the structural model of PbO NPs with the lowest toxicity was obtained.

2.3. Multiple Nonlinear Regression Analysis

Based on the linear regression, the nonlinear regression method was used to research the QSAR model. The research method in the article is the gene expression programming (GEP). GEP is a novel adaptive evolutionary algorithm based on the invention of biological gene structure and function. The basic steps of GEP nonlinear fitting are as follows.

First, within the 21 metal oxide NPs, Mn_2O_3, V_2O_3,

2019@ The American Computational Science Society. All rights reserved.

MgO and CuO were chose randomly as the test set, and the rest were chose as the training set. The 21 metal oxide NPs were randomly grouped to obtain the training set with a sample size of 17 and the test set with a sample size of 4. Then, the training set and test set were imported into the automatic problem solver (APS) software for nonlinear calculation. APS software is developed based on GEP algorithm. It allows easy optimization of intermediate solutions and easy testing of the evolved models against a test set [33].

3. Results and Discussion

3.1. Results of MLR Analysis

We used the Box-Cox transformation and stepwise regression method to establish the MLR model and obtain the toxicity prediction equation. The equation with 5 descriptors is presented in Equation (1). The 5 descriptors are X_c, *Shift*, E_g, *ZPVE, and Softness*. The values of the 5 descriptors of 21 metal oxide NPs are summarized in Table 3.

$$\ln(\log_{10}((LC_{50})^{-1})) = -0.600 + 0.743 \times x_1 + 4.413 \times x_2 - 2.688 \times x_3 - 0.000003 \times x_4 - 0.042 \times x_5 \quad (1)$$

In Equation (1), x_1, x_2, x_3, x_4 and x_5 represent X_c, *Shift*, E_g, *ZPVE*, and *Softness* respectively.

R^2 of the MLR model is 0.893. It is believed that the model is correlated if the value of R^2 is between 0.64-1. The predicted values and experimental values of 21 metal oxide NPs are summarized in Table 5. And the line graph of the experimental and predicted values of $\ln(\log_{10}((LC_{50})^{-1}))$ is shown in Figure 1. The fitted line graph with error bars of the experimental and predicted values of $\ln(\log_{10}((LC_{50})^{-1}))$ is shown in Figure 2.

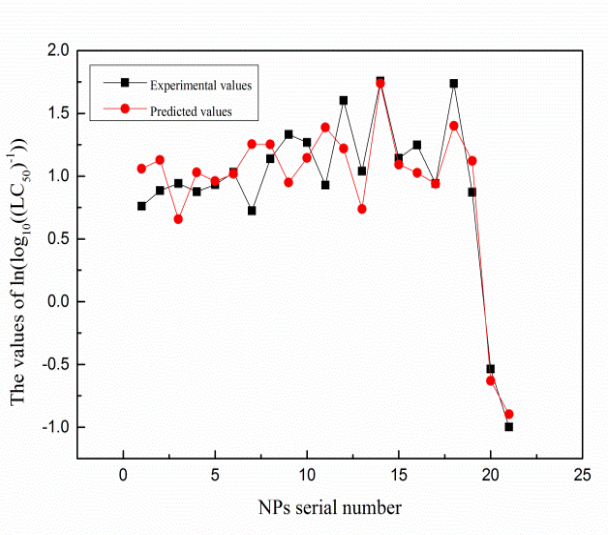

Figure 1. Two line graphs of experimental and predicted values.

Table 5. Experimental Values And Predicted Values Of Toxicity And Theri Residuals

NPs	Experimental value of $\ln(\log_{10}((LC_{50})^{-1}))$	Predicted value of $\ln(\log_{10}((LC_{50})^{-1}))$	Residual	95% Confidence interval
TiO_2	0.761	1.058	-0.297	(0.932,1.183)
Al_2O_3	0.884	1.128	-0.244	(0.953,1.303)
ZrO_2	0.940	0.657	0.283	(0.427,0.888)
Y_2O_3	0.875	1.029	-0.154	(0.739,1.320)
Cr_2O_3	0.932	0.960	-0.028	(0.827,1.093)
Sb_2O_3	1.030	1.018	0.012	(0.894,1.142)
NiO	0.723	1.254	-0.531	(1.039,1.470)
Bi_2O_3	1.138	1.252	-0.114	(1.081,1.423)
SnO_2	1.332	0.949	0.383	(0.695,1.202)
In_2O_3	1.267	1.145	0.122	(0.991,1.230)
ZnO	0.928	1.388	-0.460	(1.332,1.632)
CoO	1.601	1.219	0.382	(1.013,1.424)
V_2O_3	1.040	0.738	0.302	(0.468,1.007)
Mn_2O_3	1.756	1.737	0.019	(1.221,2.253)
CuO	1.141	1.092	0.049	(0.876,1.309)
Fe_2O_3	1.247	1.026	0.221	(0.887,1.166)
SiO_2	0.940	0.939	0.001	(0.613,1.264)
La_2O_3	1.737	1.400	0.337	(1.086,1.714)
WO_3	0.871	1.121	-0.250	(0.981,1.261)

2019@ The American Computational Science Society. All rights reserved.

MgO	-0.536	-0.629	0.093	(-1.010,-0.087)
CaO	-0.997	-0.896	-0.101	(-1.378,-0.414)

Table 6. Coefficient, Coefficient Standard Errors, P Values And VIF Values Of MLR Model

Coefficient term	Coefficient	Coefficient standard error	95% Confidence interval	P value	VIF
X_c	0.743	0.258	(0.193, 1.293)	0.011	1.910
Shift	4.413	0.656	(3.015, 5.812)	0.000	3.630
E_g	-2.688	0.630	(-4.030, -1.345)	0.001	3.120
ZPVE	-0.000003	0.000001	(-0.000005, -0.000001)	0.009	1.110
Softness	-0.042	0.009	(-0.062, -0.023)	0.000	1.060

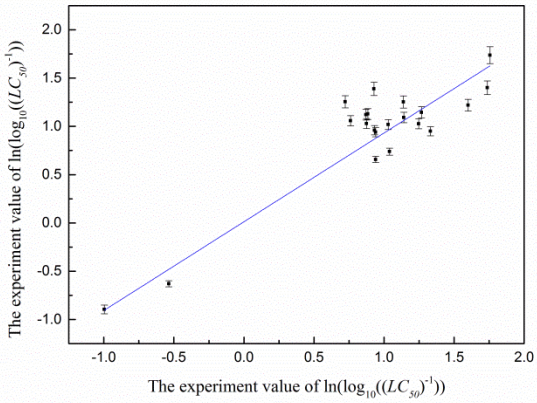

Figure 2. Fitted line graph with error bars of the experimental and predicted values of $\ln(\log_{10}((LC_{50})^{-1}))$.

3.2. Inspection of MLR model

The coefficients, coefficient standard errors, P values, and variance inflation factors (VIF) values are listed in Table 6. The P value is defined as the probability that the null hypothesis is established when the null hypothesis is true, and it is often adopted to determine whether the variable is significant. The variables are statistically significant if the P values are between 0 and 0.05 [34]. In the article, P values of the 5 descriptors are 0.011 for X_c, 0.000 for *Shift*, 0.001 for E_g, 0.009 for *ZPVE* and 0.000 for *Softness*, which show the 5 descriptors are highly significant.

VIF values of the 5 descriptors are 1.910 for X_c, 3.630 for *Shift*, 3.120 for E_g, 1.110 for *ZPVE* and 1.060 for *Softness*. If VIF values are between 1 and 5, there are no significant autocorrelation in the variables. VIF values of the 5 descriptors are all distributed within intervals 1-5, indicating that the variables in the MLR model are almost irrelevant and there is no collinearity. So it can be concluded that the MLR model is highly stable [35]. R^2 of the model is 0.893, which indicates that the experimental values have a high correlation with the predicted values. Combined with P values and VIF values, it can be concluded that the MLR model has high confidence level and has good prediction ability.

3.3. Results of the Structural Design of Ag2O3/ PbO NPs with Low Toxicity

3.3.1. Results of the structural design of Ag2O3 NPs

8 kinds of Ag_2O_3 NPs with different structures but the same number of silver atoms were submitted in Gaussian software for optimization and frequency calculation. And these 5 descriptors were calculated and were substituted into equation (1) to obtain the structural model with the lowest toxicity. Values of X_c, *Shift*, E_g, *ZPVE*, and *Softness* as well as the predicted values of $\ln(\log_{10}((LC_{50})^{-1}))$ are listed in Table 7. The value of $\ln(\log_{10}((LC_{50})^{-1}))$ is negatively correlated with the value of LC_{50}. The smaller the value of LC_{50}, the higher the toxicity. So the value of $\ln(\log_{10}((LC_{50})^{-1}))$ is positively correlated with toxicity. It can be seen from Table VII that among the 8 kinds of Ag_2O_3 NPs, the No. 4 Ag_2O_3 NPs has the minimum value of $\ln(\log_{10}((LC_{50})^{-1}))$, so it has the lowest toxicity. The structural model of No. 4 Ag_2O_3 NPs is shown in Figure 3. And the influence of each variable on toxicity are as follows: (1) X_c is positively related to the ability of Ag_2O_3 NPs to attract electrons. The larger the X_c is, the easier the ROS is produced, which causes higher toxicity. (2) *Shift* has a positive correlation with the activity of Ag_2O_3 NPs, so *Shift* has a positive correlation with toxicity. (3) The larger the E_g, the larger the energy barrier for the molecular transition, and the more stable the molecule, which leads to lower toxicity. (4) The smaller the *ZPVE*, the smaller the ground state energy of the Ag_2O_3 NPs, and the easier it is to produce ROS, resulting in higher toxicity. (5) The smaller the *softness*, the greater the polarity of Ag_2O_3 NPs, and the toxicity would be higher. These can help us understand why No. 4 Ag_2O_3 NPs has the lowest toxicity.

Table 7. Summary Of The Values Of The 5 Descriptors And The Calculated Toxicity Data Of 8 Kinds Of Silver Oxide NPs

2019@ The American Computational Science Society. All rights reserved.

Ag_2O_3 NPs	X_c	*Shift*	E_g	*ZPVE*	*Softness*	$\ln(\log_{10}((LC_{50})^{-1}))$
No. 1	2.730	-0.220	-0.054	57961.400	-0.330	0.443
No. 2	2.730	-0.224	-0.043	59028.300	-0.330	0.392
No. 3	2.730	-0.235	-0.031	59217.700	-0.330	0.311
No. 4	2.730	-0.260	-0.054	59497.600	-0.330	0.262
No. 5	2.730	-0.243	-0.035	56293.800	-0.330	0.295
No. 6	2.730	-0.251	-0.050	65635.400	-0.330	0.272
No. 7	2.730	-0.218	-0.059	60914.300	-0.330	0.456
No. 8	2.730	-0.244	-0.042	65377.100	-0.330	0.282

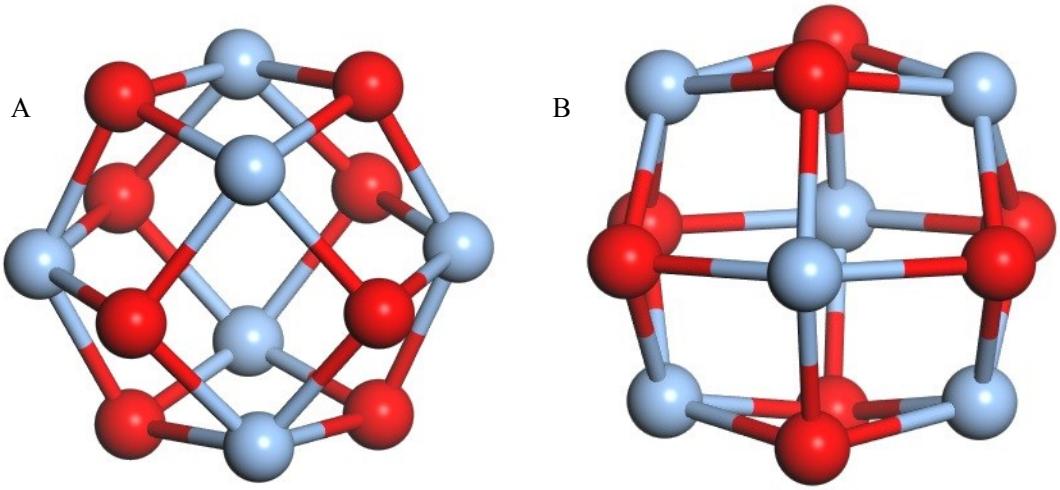

Figre 3. Structural model of Ag_2O_3 NPs with the lowest toxicity. Red balls represent oxygen atoms and light blue balls represent silver atoms. (A) shows the vertical view, (B) shows the side view.

Based on the structure of No. 4 Ag_2O_3 NPs, we discussed the relationship between the number of silver atoms and the toxicity. The calculated results of a series of Ag_2O_3 structural models with different numbers of silver atoms (2/4/6/8/10/12) are listed in Table 8. It can be seen from Table VIII that the structural model with 12 silver atoms has the lowest toxicity and the structural model is shown in Figure 4. The toxic mechanism may be that Ag_2O_3 NPs which have fewer silver atoms are smaller and more likely to pass through the phospholipid bilayer, which makes it easier to cross the cell membrane and karyotheca to damage DNA, and produce genotoxicity. Smaller Ag_2O_3 NPs can also cross the mitochondrial membrane and enter the mitochondria, leading to a decrease in mitochondrial membrane potential and cell activity. These lead to cell death eventually. H Negi et al. [36] proved through experiments that the toxicity of silver oxide NPs had a positive correlation with the specific surface area. The reason is that the larger the specific surface area, the more the Ag_2O_3 NPs contact the cells/ organisms. These lead to more severe cytotoxicity. The specific surface area is inversely related to the particle size, and it can be confirmed that the larger the particle size of Ag_2O_3 NPs, the lower the toxicity. The experimental results are consistent with the predicted results under the MLR model, which proves that the MLR model is reasonable in predicting the toxicity of Ag_2O_3 NPs [36]. Ag_2O_3 NPs with 12 silver atoms are harder to get into cells, so it has the lowest toxicity.

Table 8. Summary Of The Values Of The 5 Descriptors And The Calculated Toxicity Data Of 6 Kinds of Silver Oxide NPs With Different Numbers Of Silver Atoms

Silver numbers	X_c	*Shift*	E_g	*ZPVE*	*Softness*	$\ln(\log_{10}((LC_{50})^{-1}))$
2	2.730	-0.212	-0.079	11015.300	-0.330	0.685
4	2.730	-0.263	-0.043	38584.800	-0.330	0.280
6	2.730	-0.260	-0.054	59497.600	-0.330	0.262

2019@ The American Computational Science Society. All rights reserved.

8	2.730	-0.245	-0.049	72824.400	-0.330	0.275
10	2.730	-0.239	-0.048	89153.400	-0.330	0.250
12	2.730	-0.226	-0.043	113633.900	-0.330	0.220

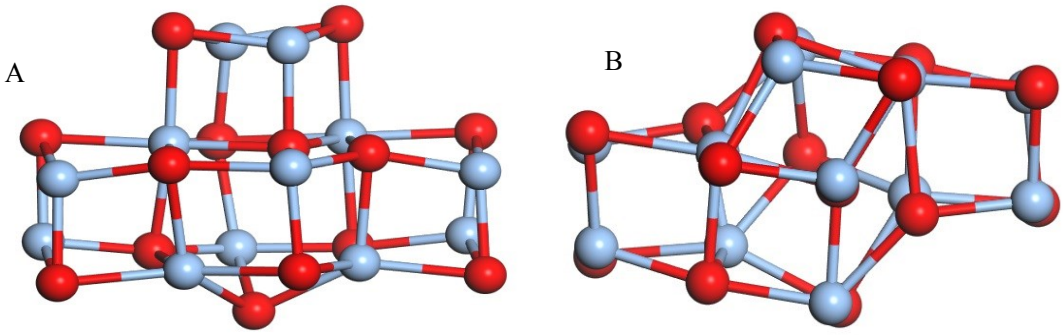

Figure 4. Structural model of Ag_2O_3 NPs with the lowest toxicity. Red balls represent oxygen atoms and light blue balls represent silver atoms. (A) shows the vertical view, (B) shows the side view.

It can be seen that Ag_2O_3 NPs with 12 silver atoms based on the structure of No. 4 Ag_2O_3 NPs has the lowest toxicity. According to the results, the number of silver atoms should be controlled around 12 based on the structural model of Figure 4 in the industrial synthesis of Ag_2O_3 NPs, so as to obtain the Ag_2O_3 NPs with the lowest toxicity.

3.3.2. Results of the structural design of PbO NPs

Similar to Ag_2O_3 NPs, the values of the 5 descriptors and the predicted toxicity data ($\ln(\log_{10}((LC_{50})^{-1}))$) of 8 kinds of PbO NPs are listed in Table 9. We can see from Table 9 that No. 6 PbO NPs has the lowest toxicity. The structural model of No. 6 PbO NPs is shown in Figure 8. Based on the structure, we studied the relationship between the toxicity and the number of metal atoms. The calculated results are listed in Table 10. It can be seen from Table X that the PbO NPs with 6 lead atoms has the lowest toxicity. We found that PbO NPs with fewer lead atoms (2/4) and more lead atoms (8/10/12) were more toxic. Experiments have also confirmed that PbO NPs with small particle size can enter cells more easily, and leading to higher toxicity [37]. The reason may be that when the number of lead atoms is fewer (2/4), PbO NPs is more likely to pass through cell membrane and karyotheca to damage DNA, thus leading to cell apoptosis and showing toxicity. However, PbO NPs with more lead atoms (8/10/12) have more sharp structures, which will rupture the cell membrane and organelle membrane, causing the cytoplasm and organelle to escape, and leading to cell death. The structural models of PbO NPs with 8/10/12 lead atoms are shown in Figure 5, Figure 6 and Figure 7 respectively. Moreover, the toxicity of PbO NPs is also manifested in the accumulation of lead in cells and organisms [38]. This weakens the effect of the number of atoms on the toxicity.

Table 9. Summary Of The Values Of The 5 Descriptors and The Calculated Toxicity Data Of 8 Kinds Of Lead Oxide NPs

PbO NPs	X_c	*Shift*	E_g	*ZPVE*	*Softness*	$\ln(\log_{10}((LC_{50})^{-1}))$
No. 1	2.831	-0.136	-0.172	49335.800	-0.250	1.211
No. 2	2.831	-0.140	-0.130	46522.800	-0.250	1.085
No. 3	2.831	-0.135	-0.173	49365.400	-0.250	1.214
No. 4	2.831	-0.138	-0.068	44859.200	-0.250	0.932
No. 5	2.831	-0.180	-0.154	63775.700	-0.250	0.921
No. 6	2.831	-0.197	-0.142	68607.000	-0.250	0.799
No. 7	2.831	-0.149	-0.146	47239.800	-0.250	1.086
No. 8	2.831	-0.173	-0.126	62018.200	-0.250	0.882

2019@ The American Computational Science Society. All rights reserved.

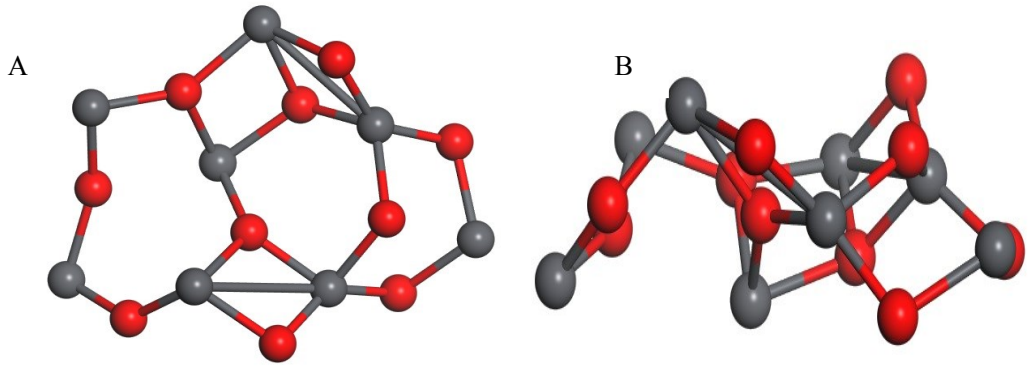

Figure 5. Structural model of PbO NPs with the 8 lead atoms. Red balls represent oxygen atoms and grey balls represent lead atoms. (A) shows the vertical view, (B) shows the side view.

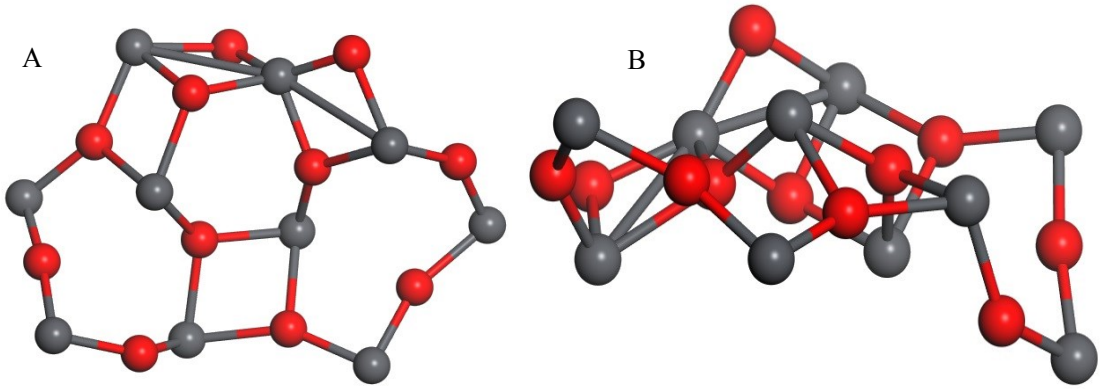

Figure 6. Structural model of PbO NPs with the 10 lead atoms. Red balls represent oxygen atoms and grey balls represent lead atoms. (A) shows the vertical view, (B) shows the side view.

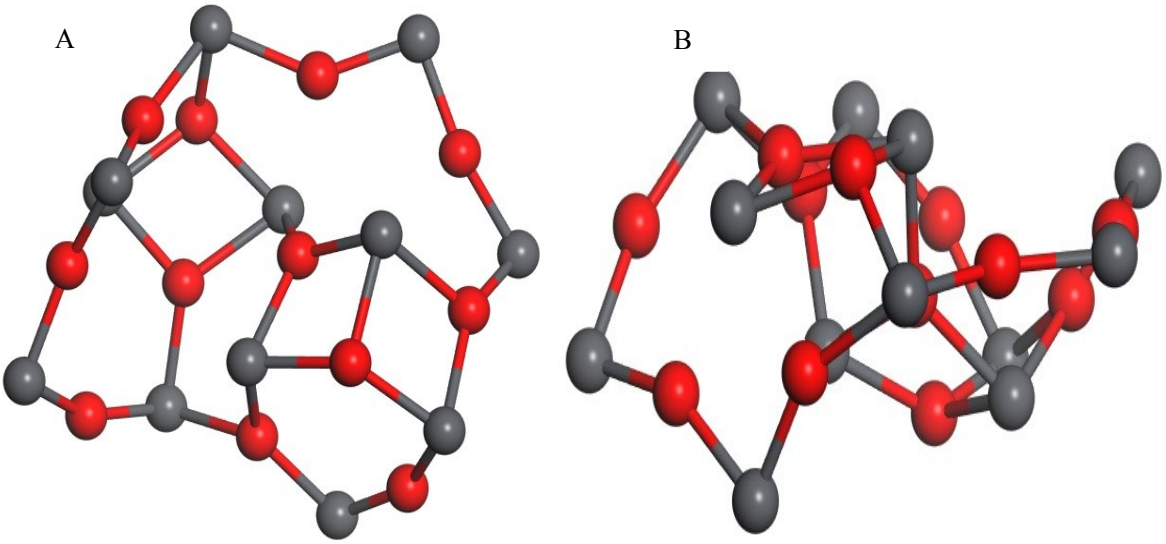

Figure 7. Structural model of PbO NPs with the 12 lead atoms. Red balls represent oxygen atoms and grey balls represent lead atoms. (A) shows the vertical view, (B) shows the side view.

2019@ The American Computational Science Society. All rights reserved.

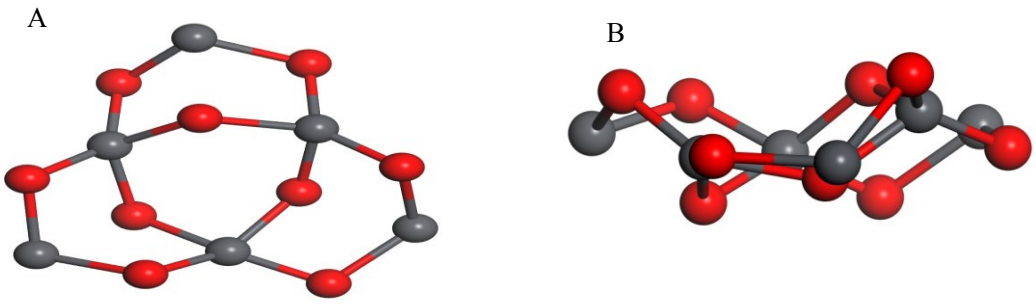

Figure 8. Structural model of PbO NPs with the lowest toxicity. Red balls represent oxygen atoms and grey balls represent lead atoms. (A) shows the vertical view, (B) shows the side view.

Table 10. Summary Of The Values Of The 5 Descriptors And The Calculated Toxicity Data Of 6 Kinds Of Lead Oxide NPs With Different Numbers Of Lead Atoms

Lead numbers	X_c	*Shift*	E_g	*ZPVE*	*Softness*	$\ln(\log_{10}((LC_{50})^{-1}))$
2	2.831	-0.155	-0.142	13432.500	-0.2500	1.150
4	2.831	-0.157	-0.153	38277.600	-0.250	1.096
6	2.831	-0.197	-0.142	68606.100	-0.250	0.799
8	2.831	-0.161	-0.137	77971.800	-0.250	0.917
10	2.831	-0.143	-0.135	85707.800	-0.250	0.968
12	2.831	-0.132	-0.121	95505.200	-0.250	0.949

In addition, the concentration of PbO NPs also have a significant effect on toxicity. M. P. Dieter et al. [39] conducted toxicity experiments on PbO NPs in rats and found that when the concentration of PbO NPs increased from 30 ppm to 100 ppm, the blood lead concentration in the rats increased from 20 μg/dL to 78.4 μg/dL. In contrast, the effect of PbO NPs with different particle sizes on blood lead concentration in rats was not significant, which proved that the main factor influencing the toxicity of PbO NPs was the concentration of PbO NPs. This experimental report also weakened the influence of particle size on toxicity. And the reason why PbO NPs with 6 lead atoms has the lowest toxicity are as follows: (1) The large volume compared with PbO NPs with 2/4 lead atoms makes it difficult to pass through the cell membrane. (2) The smoother structure compared with PbO NPs with 8/10/12 lead atoms is less likely to damage cell membrane, organelle membrane and nuclear membrane. Therefore, PbO NPs with six lead atoms has the lowest toxicity.

According to the results, the number of lead atoms should be controlled around 6 based on the structural model of Figure 8 in the industrial synthesis of PbO NPs, so as to obtain the PbO NPs with the lowest toxicity.

3.4. Multiple nonlinear regression analysis

We imported five descriptors (X_c, *Shift*, E_g, *ZPVE*, *Softness*) and toxicity data ($\ln(\log_{10}((LC_{50})^{-1}))$) into the APS software for multiple nonlinear regression calculation. The functions we chose were plus, minus, multiply, divide, absolute value, reciprocal, inverse, sine, cosine, tangent and power. And a new equation for the relationship between the 5 descriptors and the values of $\ln(\log_{10}((LC_{50})^{-1}))$ was obtained in APS software. It is presented in Equation (2).

$$\ln(\log_{10}((LC_{50})^{-1})) = x_2/(|x_1+x_2|\times 1/(\tan(1/\cos x_1))+\sin(\sin x_2) +(\sin(x_2/((\sin x_4)^{10}))/x_3^{10}+1/\cos(\tan x_5)\times(-\sin(1/\sin(2\times x_4)) +\tan(x_2\times(1/(\cos(\tan(1/(\sin(x_4\times x_5)))))))) \quad (2)$$

In Equation (2), x_1, x_2, x_3, x_4 and x_5 represent X_c, *Shift*, E_g, *ZPVE*, and *Softness* respectively.

The values of R^2 are 0.943 in training set and 0.931 in test set, which have a better prediction ability comparing with MLR model.

The predicted values of $\ln(\log_{10}((LC_{50})^{-1}))$ calculated by (2) are shown in Table 11. And the results of variance analysis of multiple nonlinear regression model are shown in Table 12. And the line graph of the experimental and predicted values of $\ln(\log_{10}((LC_{50})^{-1}))$ is shown in Figure 9. The fitted line graph with error bars of the experimental and predicted values of $\ln(\log_{10}((LC_{50})^{-1}))$ is shown in Figure 10.

2019@ The American Computational Science Society. All rights reserved.

Table 11. Experimental And Predicted Values Of Multiple Nonlinear Regression Analysis Results, And Residuals Between Them

NPs	Experimental value of $\ln(\log_{10}((LC_{50})^{-1}))$	Predicted value of $\ln(\log_{10}((LC_{50})^{-1}))$	Residual
TiO_2	0.761	0.948	0.187
Al_2O_3	0.884	0.924	0.040
ZrO_2	0.940	0.995	0.055
Y_2O_3	0.875	1.079	0.204
Cr_2O_3	0.932	0.794	-0.138
Sb_2O_3	1.030	1.141	0.111
NiO	0.723	1.015	0.292
Bi_2O_3	1.138	1.013	-0.125
SnO_2	1.332	0.824	-0.508
In_2O_3	1.267	0.965	-0.302
ZnO	0.928	1.799	0.871
CoO	1.601	1.219	-0.382
V_2O_3	1.040	1.048	0.008
Mn_2O_3	1.756	1.034	-0.722
CuO	1.141	0.966	-0.175
Fe_2O_3	1.247	0.943	-0.304
SiO_2	0.940	1.010	0.070
La_2O_3	1.737	1.478	-0.259
WO_3	0.871	1.145	0.274
MgO	-0.536	0.641	1.177
CaO	-0.997	-1.016	-0.019

Table 12. Equation Analysis Of Training Set And Test Set

Sample	MSE Value	R^2
Training Set	0.018	0.943
Test Set	0.482	0.931

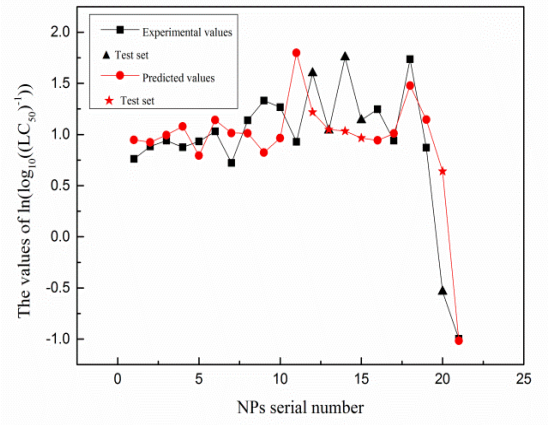

Figure 9. Line graphs of experimental and predicted values.

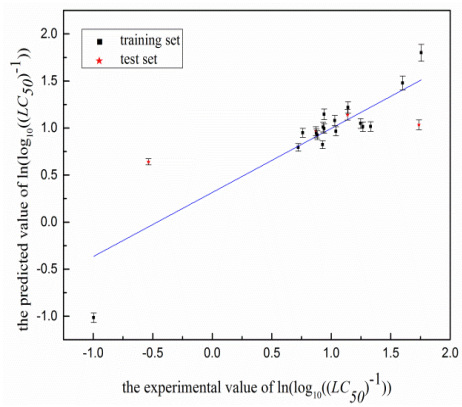

Figure 10. Fitted line graph of the experimental and predicted values of $\ln(\log_{10}((LC_{50})^{-1}))$.

2019@ The American Computational Science Society. All rights reserved.

The error parameter listed in Table 12 is the mean squared errors (MSE). MSE characterizes the deviation between experimental values and predicted values. If the absolute values of the MSE are closer to zero, the prediction ability of the model would be better. The predicted values were calculated by (2). It can be seen from Table 12 that the values of the MSE are 0.018 for training set and 0.482 for test set, indicating that the multiple nonlinear regression model has good stability and high credibility.

Table 13. Summary Of The Values Of The Remaining 20 Descriptors Of 21 Kinds Of Metal Oxide NPs

NPs	$\Delta_f H^0$	$\Delta_f G^0$	*HOMO*	*LUMO*	C_p
TiO_2	-944.0	-888.80	-0.164	-0.098	55.480
Al_2O_3	1675.7	-1582.30	-0.299	-0.127	79.040
ZrO_2	-1100.6	-1042.80	-0.121	-0.086	56.190
Y_2O_3	-1905.3	-1816.60	-0.239	-0.073	102.510
Cr_2O_3	-1139.7	-1058.10	-0.199	-0.127	118.740
Sb_2O_3	-971.9	-829.20	-0.218	-0.143	101.630
NiO	-489.5	-571.32	-0.149	-0.113	44.310
Bi_2O_3	-573.9	-493.70	-0.251	-0.077	113.510
SnO_2	-577.6	-515.80	-0.229	-0.144	52.590
In_2O_3	-925.8	-830.70	-0.271	-0.149	92.000
ZnO	-350.5	-320.50	-0.148	-0.085	40.250
CoO	-237.9	-214.20	-0.201	-0.100	55.230
V_2O_3	-1218.8	-1139.30	-0.193	-0.101	103.220
Mn_2O_3	-959.0	-881.10	-0.207	-0.136	117.540
CuO	-157.3	-129.70	-0.217	-0.176	42.300
Fe_2O_3	-824.2	-742.20	-0.232	-0.148	103.850
SiO_2	-910.7	-856.30	-0.206	-0.074	44.130
La_2O_3	-1793.7	-1705.80	-0.095	-0.097	108.780
WO_3	-842.9	-764.00	-0.182	-0.132	110.020
MgO	-601.6	-569.30	-0.798	-0.053	37.200
CaO	-634.9	-603.30	-0.100	-0.061	42.000

Continue…

NPs	*Hard*	*G*	*ΔH*	E_{TH}	*ZPE*
TiO_2	2.140	-5850.826	-5850.751	-5850.752	-5850.774
Al_2O_3	5.090	-2208.953	-2208.890	-2208.891	-2208.909
ZrO_2	5.970	-1185.873	-1185.795	-1185.796	-1185.821
Y_2O_3	1.840	-982.424	-982.346	-982.347	-982.369
Cr_2O_3	2.830	-7020.069	-7020.000	-7020.001	-7020.021
Sb_2O_3	3.500	-786.188	-786.111	-786.112	-786.134
NiO	3.040	-9500.173	-9500.120	-9500.121	-9500.134
Bi_2O_3	4.090	-786.536	-786.454	-786.455	-786.478
SnO_2	2.400	-1079.756	-1079.664	-1079.665	-1079.694
In_2O_3	3.840	-765.253	-765.173	-765.174	-765.197
ZnO	3.030	-11126.347	-11126.288	-11126.287	-11126.304
CoO	3.430	-8747.051	-8746.997	-8746.998	-8747.012
V_2O_3	4.040	-6417.751	-6417.687	-6417.688	-6417.707
Mn_2O_3	0.020	-7658.894	-7658.824	-7658.824	-7658.844
CuO	2.980	-10293.090	-10293.033	-10293.034	-10293.049

2019@ The American Computational Science Society. All rights reserved.

Fe_2O_3	4.440	-8335.010	-8334.942	-8334.943	-8334.962
SiO_2	4.090	-2932.347	-2932.269	-2932.270	-2932.293
La_2O_3	4.450	-866.105	-866.024	-866.025	-866.047
WO_3	0.110	-1445.994	-1445.903	-1445.904	-1445.931
MgO	5.500	-10465.227	-10465.137	-10465.318	-10465.172
CaO	3.500	-3780.822	-3780.747	-3780.748	-3780.776

Continue…

NPs	C_V	*E*	*DM*	μ	*ds*
TiO_2	73.229	-5850.831	0.004	-0.441	9.134
Al_2O_3	65.075	-2208.977	1.839	-0.503	6.871
ZrO_2	89.380	-1185.904	0.023	-0.798	9.033
Y_2O_3	76.551	-982.423	0.006	-0.687	8.191
Cr_2O_3	70.208	-7020.082	3.786	-0.501	7.265
Sb_2O_3	74.911	-786.189	3.894	-0.717	9.416
NiO	44.003	-9500.160	0.000	-0.098	4.315
Bi_2O_3	75.044	-786.531	3.801	-0.717	9.625
SnO_2	101.744	-1079.783	6.577	-0.488	6.466
In_2O_3	78.369	-765.249	2.331	-0.718	7.866
ZnO	50.164	-11126.327	0.000	-0.161	4.168
CoO	50.284	-8747.038	0.000	-0.100	7.867
V_2O_3	68.768	-6417.770	5.327	-0.532	7.489
Mn_2O_3	69.763	-7658.905	1.677	-0.399	7.052
CuO	48.845	-10293.071	0.000	-0.065	4.315
Fe_2O_3	67.670	-8335.026	5.543	-0.370	7.560
SiO_2	81.688	-2932.394	5.143	-0.319	6.497
La_2O_3	72.387	-866.083	5.445	-0.141	9.999
WO_3	88.453	-1445.973	0.115	-1.471	3.480
MgO	127.793	-10465.226	0.000	-0.492	4.168
CaO	116.156	-3780.843	0.000	-0.013	4.211

Continue…

NPs	*dw*	*V*	*T*	ρ	*refractive index*
TiO_2	2.015	72.773	2143	3.900	2.350
Al_2O_3	1.863	50.959	2372	3.700	1.630
ZrO_2	9.033	79.786	2973	5.850	2.050
Y_2O_3	2.409	98.384	2712	5.030	1.800
Cr_2O_3	2.020	62.722	2708	5.210	2.551
Sb_2O_3	2.159	73.246	929	5.600	2.090
NiO	4.315	80.342	2253	6.840	2.182
Bi_2O_3	4.613	94.883	1097	8.900	1.910
SnO_2	6.895	335.621	1903	6.950	1.977
In_2O_3	2.094	59.152	2273	7.179	4.700
ZnO	4.168	72.407	2248	5.606	2.010
CoO	3.368	52.171	2208	6.450	1.740
V_2O_3	1.961	61.314	2243	4.870	1.520

2019@ The American Computational Science Society. All rights reserved.

Mn_2O_3	2.024	60.775	1353	4.500	2.400
CuO	4.315	80.342	1299	6.600	2.630
Fe_2O_3	1.950	62.875	1838	5.240	3.010
SiO_2	5.918	249.805	1923	2.200	1.460
La_2O_3	2.849	84.319	2588	6.510	1.580
WO_3	3.479	42.192	1745	7.160	1.368
MgO	4.168	72.407	2845	3.350	1.838
CaO	4.211	74.672	3073	3.530	1.700

Table 14. Summary Of The Dfinations And Physical Meanings Of The 25 Descriptors

Descriptors	Defination and physical meaning
$\Delta_f H^0$	Standard molar enthalpy (heat) of formation at 298.15 K in J/mol
$\Delta_f G^0$	Standard molar Gibbs energy of formation at 298.15 K in J/mol
HOMO	The highest occupied orbital energy at 298.15 K in J/mol
LUMO	Lowest occupied orbital energy at 298.15 K in J/mol
C_p	Molar heat capacity at constant pressure at 298.15 K in J/mol K
Hard	Chemical hardness based on the Hard-Soft-Acid-Base theory (HSAB) at 298.15 K in J/mol
G	Sum of electronic and thermal Free Energies at 298.15 K in J/mol
ΔH	Standard molar enthalpies of formation at 298.15 K in J/mol
E_{TH}	Sum of electronic and thermal Energy at 298.15 K in J/mol
ZPE	Sum of electronic and zero-point Energy at 298.15 K in J/mol
C_V	Molar heat capacity at constant volume at 298.15 K in J/mol K
E	Total energy of the nanoparticle system at 298.15 K in J/mol K
DM	Dipole moment (dimensionless)
μ	Electron chemical potential at 298.15 K in J/mol K
ds	The length of a nanoparticle, the unit is angstroms
dw	The width of a nanoparticle, the unit is angstroms
V	The volume of nanoparticles
T	Fusion point at Standard atmospheric pressure in K
ρ	Density, the unit is kg/m^3
refractive index	Refractive index (dimensionless)
X_c	Electronegativity (Relative scale)
Shift	The half of the sum of the highest occupied orbital energy and the lowest unoccupied orbital energy
E_g	the difference between the Homo and the Lumo (band gap) at 298.15 K in J/mol
ZPVE	Zero-point vibrational energy at 298.15 K in J/mol K
Softness	The Chemical softness based on the Hard-Soft-Acid-Base theory (HSAB) at 298.15 K in J/mol

4. Conclusion

In the article, the quantitative relationship between toxicity and structures of metal oxide NPs is researched by using QSAR model. Equations between descriptors and toxicity data LC_{50} were established. It indictes that the values of LC_{50} is related to 5 descriptors (X_c, *Shift,* E_g, *ZPVE, and Softness*). Based on MLR regression equation, the structures of silver oxide and lead oxide with the lowest toxicity were designed, and further discussed the effect of the number of metal atoms on toxicity. Multiple nonlinear regression models were adopted for further research, and the prediction equation was obtained. The result indicted that the

2019@ The American Computational Science Society. All rights reserved.

multiple nonlinear regression model improved the prediction accuracy of the QSAR model. The mechanisms that the 5 descriptors affect the toxicity of metal oxide NPs were further discussed. It is concluded that metal oxide NPs could promote the generation of ROS through a series of complex chemical reactions, thus showing toxicity. These conclusions have significant implications for understanding the toxicity mechanisms of metal oxide NPs, predicting the toxicity of unknown metal oxide NPs and reducing their toxicity.

References

[1] H. Zhang, Z. Ji, T. Xia et al. American Chemical Society 6(2012) 4349-4368.
[2] S. Park, H. Chibli, J. Wong, J. L. Nadeau. Nanotechnology, 22(2011).
[3] C. Migdal, R. Rahal, A. Rubod, S. Callejon, E. Colomb, N. Atrux-Tallau. Toxicology Letters, 199(2010) 34-42.
[4] T. Puzyn, D. Leszcynska, J. Leszcynski. Small, 5(2009) 2494-2509.
[5] D. Fourches, D. Pu, A. Tropsha. Comb Chemistry High Tscr, 14(2011) 217-225.
A. Gajewicz, N. Schaeublin, B. Rasulev, S. Hussain, et al. Nanotoxicology, 9(2014) 313-325.
[6] L. K. Adams, D. Y. Lyon, P. J. J. Alvarez. Water Research, 40(2006) 3527-3532.
[7] A. Minigalieva, B. A. Katsnelson, V. G. Panov, L. I. Privalova et al. Toxicology, 380(2017) 72-93.
[8] V. Aruoja, H. C. Dubourguier, K. Kasemets, Kahru. Total Environ, 407(2009) 1461-1468.
[9] Y. W. Baek, Y. J. An. Science of the Total Environment, 409(2011) 1603-1608.
[10] H. L. Karlsson, J. Gustafsson, P. Cronholm, L. Möller. Toxicology Letters, 188(2009) 112-118.
[11] L. Liu, Y. Zhao, B. Sun, C. Chen. Accounts of Chemical Research, 46(2013) 702-713.
A. Semisch, J. Ohle, B. Witt, A. Hartwig. Particle and Fibre Toxicology, 11(2014) 1-1.
[12] P. Chairuangkitti, S. Lawanprasert, S. Roytrakul. Toxicology in Vitro, 27(2012) 330-338..
[13] C. M. Sayes, F. Liang, J. L. Hudson, J. Mendez, W. Guo. Toxicology Letters, 161(2016) 135-142.
[14] C. M. Lin, C. T. Chen, H. H. Lee et al. Planta medica, 68(2002) 365-7.
[15] L. T. Qin, S. S. Liu, F. Chen, Q. F. Xiao, Q. S. Wu. Chemosphere, 90(2013) 300-305.
[16] D. Wang, J. Yu, Y. Gao, L. Zh, Z. Lin, D. Yin. Journal of Safety and Environment, 12(2012).
[17] S. Kim, E. Kuk, K. N. Yu. Biology and Medicine, 3(2007) 95-101.
[18] M. Karelson, V. S. Lobanov, A. R. Katritzky. Chemical reviews, 96(1996) 1027-1044.
[19] D. Urbisch, N. Honarvar, S. N. Kolle, A. Mehling, T. Ramirez et al. Toxicology in Vitro, 34(2016) 194-203.
[20] T. Puzyn, B. Rasulev, A. Gajewicz, X. Hu, et al. Nature Nanotechnology, 6(2011) 175-178.
[21] R. Liu, H. Zhang, Z. Ji, et al. Nanoscale, 5(2013) 5644-5653.
[22] N. N. Mrabti, M. Elhallaoui et al. Journal of Taibah University for Science, 11(2016) 18-39.
[23] X. Hu, S. Cook, P. Wang, H. Hwang. Science of the Total Environment, 407(2009) 3070-3072.
A. Soffers, M. G. Boersma, W. H. J. Vaes et al. Toxicology in Vitro, 15(2001) 539-551.
[24] R. G. Pearson. ACS Publications, 45(1968) 581-581.
[25] Ying. Eastsouth University, 2006.
[26] Pathakoti, M. G. Huang, J. D. Watts, et al. Journal of Photochemistry and Photobiology B: Biology, 130(2014) 234-240.
[27] Ghobadian, M. Nabiuni, K. Parivar, et al. Ecotoxicology and Environmental Safety, 122, (2015) 260-267.
[28] J. A. Kovrižnych, R. Sotníková, D. Zeljenková, et al. Toxicology, 6(2013) 67–73.
[29] A, A. Olajire, E. A. Oluyemi, E. T. Ayodele et al. Taylor & Francis, 15(2007) 151-158.
[30] H. Z. Si, K. J. Zhang, Z. D. Hu et al. QSAR & Combinatorial, 26(2007) 41-50.
[31] J. P. T. Higgins, G. Simon, Thompson. Statistics in Medicine, 21(2002) 1539-1558.
[32] R. M. O'brien. Quality & Quantity, 41(2017) 673-690.
[33] H. Negi, P. R. Saravanan, T. Agarwal. The Journal of General and Applied Microbiology, 59(2012) 83-88.
[34] A Seaton, K Donaldson. The Lancet, 365(2005) 923-924.
[35] S. V. Verstraeten, L. Aimo, P. I. Oteiza. Archives of toxicology, 82(2008) 789-802.
[36] P. Dieter, H. B. Matthews, R. A. Jeffcoat. Journal of Toxicology and Environmental Health, 39(2009) 79-93.

2019@ The American Computational Science Society. All rights reserved.